wjpmr, 2022,8(7), 156-168

SJIF Impact Factor: 5.922

WORLD JOURNAL OF PHARMACEUTICAL AND MEDICAL RESEARCH

www.wjpmr.com

Research Article

ISSN 2455-3301

WJPMR

ROLE OF CYCLOPHOSPHAMIDE–BIOPOLYMERIC BASED COMPOSITES AGAINST NEPHROTOXICITY IN RATS

Ibrahim A. El Desoky, Eman M. Saleh, Atef S. Darwish and Rasha E. Hassan*

AIN Shams University, Faculty of Science, Biochemistry Dept.

***Corresponding Author: Rasha E. Hassan**

AIN Shams University, Faculty of Science, Biochemistry Dept.

Article Received on 20/05/2022 **Article Revised on 10/06/2022** **Article Accepted on 30/06/2022**

ABSTRACT

Cyclophosphamide (CP) is an effective anti-cancer alkylating agent, while it also possesses a wide spectrum of cytotoxicity as nephrotoxicity. Nanoparticles are used as drug carriers and imaging to increase drug solubility, stability and control drug release and specific transport and reduce drug toxicity. The current study was constructed to evaluate the ameliorating effect of the newly synthesized CP& Egg albumin /carbon nanotube nanocomposite (CP&EA/ CNT) against CP induced nephrotoxicity in rats and to investigate the effectiveness of the newly synthesized composite in treating nephrotoxicity. The physicochemical properties of the newly synthesized composite were also assessed by Characterization techniques such as TEM, SEM, zeta-potential, FT-IR and XRD. In vitro study (Cell viability assay) wherever the cytotoxic effect (IC50) of newly synthesized composite (CP&EA/CNT). To achieve this goal In vivo assay, 24 adult male rats were randomly divided into three equal groups (8 rats/group), (1) control group, (2) CP group, (3) CP&EA/CNT group. After experimental period, serum renal biomarkers (creatinine, urea, uric acid, BTP, nepherin, interleukin 8(IL8) and NGAL were evaluated. In addition, histopathological examination of kidney and was performed. Our results prove that CP caused nephrotoxicity shows increase in (creatinine, urea, uric acid, BTP, nephrin, IL8 and NGAL) levels for groups that were injected with CP only in healthy rats. Groups were injected with CP&EA/CNT nanocomposite revealed a significant improvement in renal biomarkers levels and also improve in histopathological disorders of kidney. Ultimately, the outcomes of this study ascertained the ameliorating role of the newly synthesized CP&EA/CNT nanocomposite against nephrotoxicity induced by CP in rats without interfering with CP anticancer properties.

INTRODUCTION

Acute kidney injury (AKI) is caused by a wide variety of pathogenic events, including sepsis, infection, ischemia, and drug toxicity. AKI is a severe disorder in which renal function declines rapidly and results in high mortality by multi-organ failure and sepsis. Furthermore, some patients who recovered from AKI are known to develop chronic kidney disease (CKD). At present, therapies for AKI are limited to supportive care such ashemodialysis. For this reason, several biomarkers have been investigated as early diagnostic markers of AKI severity and markers of progression to CKD (Tabata et al., 2020).

Urinary and serum/plasma Neutrophil gelatinase associated Lipocalin (NGAL) levels are elevated within 6 hour of the kidney injury, while the rise in serum creatinine levels occurs only after more than 50% of renal function is lost, which may take days. Expression of NGAL mRNA increases more than 1000-fold in response to kidney injury and manifests as rapid elevation of urine and blood NGAL levels, making it useful as an early biomarker. It has been shown that elevated NGAL predicts the development of AKI before serum creatinine in conditions such as cardiac surgery-associated AKI, after renal transplantation and AKI in the critical care setting. Studies have also demonstrated the utility of early NGAL test in predicting the prognosis of AKI (Siddappa et al., 2019).

Nephrin is a slit diaphragm protein that is critical for glomerular filtration as it provides architectural support to podocytes. Nephrin shedding is used as a marker of glomerular-specific renal damage in a variety of settings and was observed prior to the development of albuminuria in a mouse model of proteinuric renal disease. As nephrinuria develops before albuminuria, nephrin may be a suitable biomarker for early detection of glomerulopathy. As nephrin is a glomerular-specific protein, monitoring of this biomarker might be more indicative of glomerular injury than other putative biomarkers in the current literature (Heimlich et al., 2018).

IL-8 is a proinflammatory cytokine produced by monocyte, neutrophil, endothelial, and epithelial cells, and it acts as a potent neutrophil activator and chemoattractant. After ischemia- reperfusion injury, IL-8

is released by stem cells and endothelial progenitor cells into the systemic circulation, thereby increasing inflammation. Several studies have previously reported that plasma IL-8 is strongly associated with the development of AKI and other adverse outcomes after pediatric cardiac surgery. In a study on 817 critically ill adults receiving Renal replacement therapy for AKI, adding plasma IL-8 to a clinical model had predictive value for renal replacement therapy (RRT) requirement at 60 days after enrollment. IL-8 has also been reported to predict mortality in patients with AKI, but its ability to predict AKI progression has not been assessed (de Fontnouvelle et al., 2017; Greenberg et al., 2018).

Cyclophosphamide is one of the oldest anticancer drugs. It is an alkylating agent belonging to the group of oxazaphosporines. It was discovered as early as 1958 and introduced into cancer therapy in 1959. It is widely used to treat various types of cancer including lymphoma, leukemia, breast, ovarian, colon and small-cell lung carcinomas (Iqubal et al., 2020; Zhao et al., 2020). Cyclophosphamide has severe side effects including leuco- and thrombocytopenia, nephrotoxicity, cardiotoxicity, malnutrition, urotoxicity and hepatotoxicity. All these effects are highly dose dependent (Amal et al., 2020; Ayza et al., 2020; S. Jiang et al., 2020b).

In addition, one of the main mechanisms involved in nephrotoxicity is apoptosis. CP induces apoptosis of cells of kidney by induces the imbalance of apoptosis-associated proteins. CP stimulation decreases the level of antiapoptotic protein Bcl-2 and increase the level pro-apoptotic protein Bax. Bax induces the release of cytochrome C and cascade of apoptosis pathway. Also, CP provokes NF-κB led to the generations of pro-inflammatory cytokines, such as interleukin-6, interleukin-1β and tumor necrosis factor alpha (TNF-α) (ALHaithloul et al., 2019a).

The current study was constructed to evaluate the ameliorating effect of the newly synthesized cyclophosphamide-biopolymeric based composite against cyclophosphamide induced nephrotoxicity in rats. The physicochemical properties of the newly synthesized composite were also assessed.

MATERIALS

Cyclophosphamide (also it has trade name Endoxan 1gram) was purchased from (Baxter Oncology, Dusseldorf, Germany; batch no 7c117). 1,2 dimethylhydrazine (DMH), Egg albumin and Carbon Nanotube from (Sigma Aldrich Chemical Company, USA).

Methods

Preparation of nano composites (delivery systems). Cross-linked egg albumin nanoparticles (EA-NPs) were prepared by the desolvation method (Kayani et al., 2017). In this regard, one g of EA was dissolved in 50 mM NaCl solution at pH 7.0 and then incubated in a water bath at 60° C to ensure complete solubility. After that, the pH of the EA solution was adjusted to 9 using 0.1 M NaOH. Proper amount of acetone as a desolvating agent was added drop wise at a rate of 0.1 ml/min until the solution became just turbid. Afterwards a volume of 58 µl of 10 %v/v glutaraldehyde solution was added to induce particle cross-linking with continuous stirring at room temperature for 72 h. The solid fractions were washed several times by water, filtered and dried at 60o C for 6 h, and finally preserved under vacuum.

In preparing carbon nanotube (CNT) hybridized EA-NPs, the same above-mentioned procedure for egg albumin dissolution was followed. Then, appropriate amount of CNT (0.4 g) was added to the egg albumin aqueous solution and the reaction mixture was stirred for 2 h at 60o C and then 0.1 M NaOH was added drop wisely until the pH achieved 9. Glutaraldehyde solution (10 %v/v) was then added under vigorous stirring at room temperature to initiate crosslinking of egg-albumin. The black slurry was left under stirring over night at room temperature, and then washed several times by distilled water, filtered, and finally dried at 70oC for 6 h. The produced nanocomposite was preserved under vacuum and symbolized by "EA/CNT".

Characterization of newly synthesized nanocomposites. The EA-NPs and EA/CNT nanocomposites were analyzed using X-ray powder diffractometry (XRD) of Phillips model PW3710-BASED equipped with Ni-filtered Cu Ka radiation (k = 1.5418 Å), Fourier transform infrared (FTIR, ATi Mattson, WI-53717, USA) spectroscopy with a nominal resolution of 2 cm-1, scanning electron microscopy (SEM, JEOL JSM-5300) working at 30 kV, and high-resolution transmission electron microscope (HRTEM, JEOL-2100) operating at 200 kV with resolution of 0.14 nm. The zeta potentials of the understudied samples were measured by zeta sizer-Nano ZS (MALVERN, United Kingdom) as discussed elsewhere (Mekewi et al., 2015).

In vitro study

Cell lines and cell culture. The cell lines on mammary gland breast cancer cell line (MCF7) (Quaroni et al., 1979) were used in this experiment. Use of trypan blue for staining relies on the fact that live cells have intact plasma membranes that can exclude various chemicals, including trypan blue. Dead cells invariably have ruptured plasma membranes, regardless of the mechanism of death, and cannot exclude trypan blue (Kunjeti et al., 2016). Cell viability was measured by MTT assay for determination of IC50 (Twentyman & Luscombe, 1987; Saeed et al., 2017).

In vivo study

Determination of LD50 of CP& Egg albumin/Carbon nanotube nanocomposite: Preliminary experiments were carried out on 6 groups (10 rats in each group) to calculate LD50 for CP &EA/CNT nanocomposite. Rats

were intraperitoneally injected in different doses to find out the range of doses which cause zero and 100% dead of animals. A range doses was determined as follow 50, 250, 450, 650, 850, and 1050 mg/kg, ac cording to the method of Finney (1964) using the following formula:

$$LD_{50} = Dm - \frac{\sum (Z \cdot d)}{n}$$

Dm= the dose by which killed all the rats in the group.
Z = Half the sum of the dead rats from 2 successive groups.
d = the difference between 2 successive doses.
N = number of animals in each group.

Experimental animals

Twenty four adult male albino rats weighing 150-200 g were obtained from Faculty of pharmacy, Al-Azhar University. The animals were in steel cages in 6 groups of eight rats per cage. They were kept healthy under optimum conditions of temperature, humidity and 12 h photoperiod. Rats were fed a diet consisting principally of fodder and bread. They had access to tap water, in addition minerals and vitamins that added from time to time. Animal's maintenance and treatments were conducted in accordance with the National Institute of Health guide for animal as approved by institutional animal care and use committee (IACUC).

Experimental design. Twenty-four albino rats were allocated into three groups, eight animals in each group as: Group I (Normal control): Healthy rats were intraperitoneally injected with saline (20 ml /kg b.w) daily for 7 days. Group II (CP group): Healthy rats were intraperitoneally injected with CP (20 mg/kg b.w) daily for 7 days (Cuce et al., 2015). Group III (CP&EA/CNT group): Animals were intraperitoneally injected with 1/10 dose of LD50 as CP+EA/CNT nanocomposite (CP 0.007 g + EA/ CNT 0.1g per 200 g b.wt) daily for 7 days according to results obtained from IC50. At the end of the experiment, animals were weighed then were anesthetized with light diethyl ether and sacrificed after 24 h fasting period from the final administration. Blood samples were collected from the abdominal aorta for biochemical analyses and were left to clot and centrifuged at 3000 rpm for 20 min at 25°C for serum preparation. Kidney and colon tissues were removed for histopathological studies.

Biochemical analyses and Assessment of nephrotoxicity. Determination of kidney function (serum creatinine, urea, Uric acid; according to the instruction of kits). Moreover, B trace protein (BTP), that was measured according to N Latex BTP assay kit in addition to Nephrin and Interleukin 8 (IL8), in which, assay is based on the sandwich ELISA technique, as well as neutrophil gelatinase associated lipocalin (NGAL), where immunohistochemical staining procedures were done according to (Saber et al., 2019).

RESULTS

The current study was designed to evaluate the ameliorating effect of Egg albumin/ carbon nanotube composite against cyclophosphamide induced renal injury in rats.

1- Characterization of newly synthesized CP&EA/CNT composite

1-1- X-ray diffraction (XRD) analysis. The XRD patterns of EA-NPs and EA/CNT nanocomposite are represented in Fig. (1a&b). In both samples, strong broad bands extended between 10 and 500 are appeared, indicating significant amorphicity of the egg-albumin structure, whether alone or in the hybrid nanocomposite.

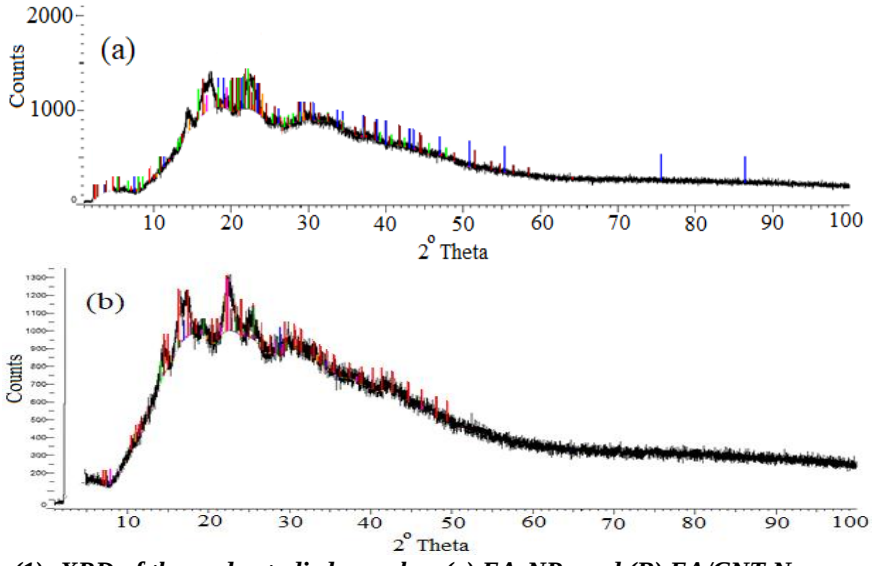

Figure (1): XRD of the understudied samples; (a) EA-NPs and (B) EA/CNT Nanocomposite

1-2- Fourier transform infrared spectroscopy (FTIR) analysis

The FTIR spectra of the as prepared samples were studied and depicted in (Fig. 2) in the spectrum of EA-NPs (Fig. 2a), there are different peaks at 750, 967, 1230, 1750, and 2933 cm−1. The peak at 750 cm−1 belongs to N-H wagging, peak at 967 cm−1 is associated to stretching of C-C, peak at 1230 cm−1 is correlated to the stretching C-N band of amide III region that is associated to presence of β-sheet conformation, peak at 1750 cm−1 is associated with C=O stretching vibration of amide I region, and peak at 2933 cm−1 indicates stretching vibration of C-H band (Sripriyalakshmi et al., 2014), (Noorani et al., 2017a). A broad band centered at 1367 cm−1 is ascribed to the bending vibration of N-H band and stretching vibration of C-N band of amide II region (Noorani et al., 2017b). Another broad band in the region 3000 - 3760 cm−1 reflects stretching vibration of OH groups (Sripriyalakshmi et al., 2014).

After hybridizing EA-NPs by carbon nanotube (Fig. 2b), red shifting in the amides I band and N-H wagging are observed, revealing intimate interaction between proteinaceous segments in the egg albumin chains and carbon nanotubes, which may cause incorporation of EA NPs within the carbon nanotubes as further shown by TEM observations. Also, broadening of the band characteristic to the stretching vibrations of OH groups is much more pronounced when compared with that of EA-NPs and shifts to lower frequency being centered at 3333 cm−1. This result confirms the significant linkage of the polypeptide chains of egg albumin with carbon nanotube.

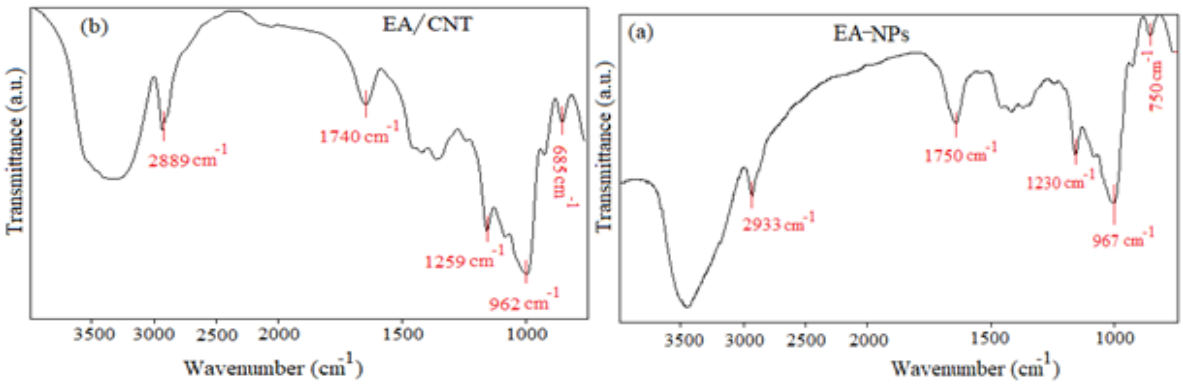

Figure (2): FT-IR of the samples under investigation ;(a) EA-NPs and (b) EA/CNT Nanocomposite.

1-3- Surface charge potential study. The zeta-potential distribution curve is presented in (Fig. 3) as shown from (Fig. 19a), the mean zeta potential of EA-NPs is well-described by negative charges pointing most probable to the enrichment of polypeptide chains of EA-NPs by various anionic species like carboxylate and phenolate anions. Such diversity in the negative character is also confirmed by the wide range of the recorded zeta-potentials from -90 mV to -20 mV. Such alteration in zeta values may reflect existence of large-sized charging particles, as the particles of large diameter may owe plenty of negative charges as evidenced in previous work (Mekewi et al., 2015). In EA/CNT nanocomposite (Fig. 19b), the formed particles exhibit lower negative mean zeta-potential (-13 mV) in comparison with that of EA, reflecting presence of protonated hydroxyls (-OH), and neutral amide and carboxylic groups in the polypeptide chains. Also, the zeta-potential curve of EA/CNT displays a sharp peak indicating presence of unimodal charged and uniformly sized particles.

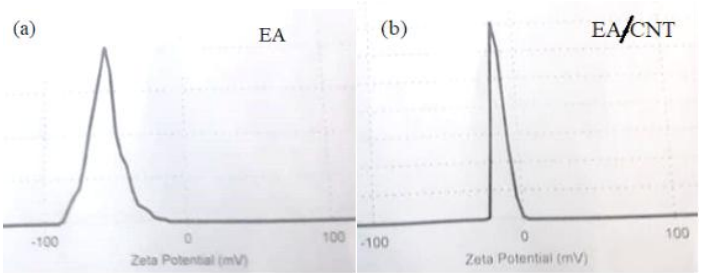

Figure (3): Zeta-potentials of samples under study; (a) EA-NPs and (B) EA/CNT composite.

1-4- Scanning electron microscope (SEM) analysis

The SEM micrographs of EA-NPs and EA/CNT are illustrated in (Fig. 4). The EA nanoparticles are aggregated forming spherical micro-sized particles (~7.5µm), and uniformly separated from each other (Fig. 4A). By hybridization of EA NPs with CNT, the spherical shape of albumin nanoparticles is highly deformed (Fig. 4B). As shown in (Fig. 4C), a dense layer of carbon nanotubes is firmly attached and radically based onto the surface of albumin aggregates. This view is in consistent with the suggested intimate albumin - carbon nanotube interactions by the FTIR study.

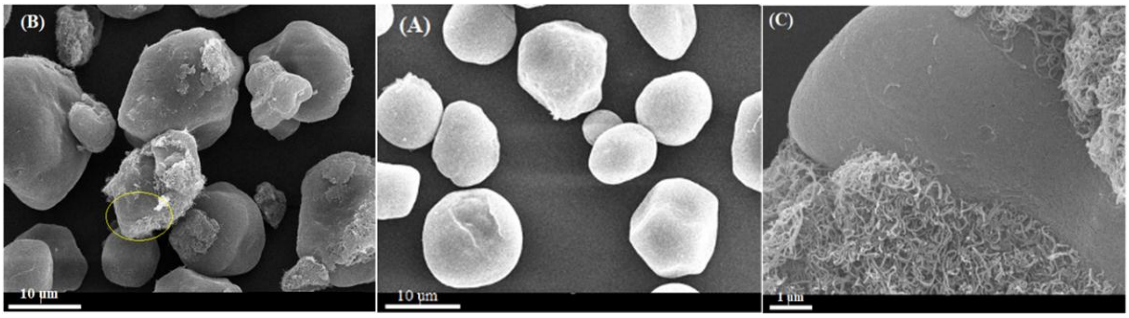

Figure (4): SEM micrographs of: (A) EA-NPs and (B and C) EA/CNT nanocomposite.

1-5- Transmission electron microscopy (TEM) analysis

The TEM images of EA-NPs and EA/CNT are represented in (Fig. 21) as can be seen in (Fig. 5A) spherical-shaped albumin nanoparticles of sizes ranged from 30 – 60 nm are formed and aggregated, as being evidenced by corresponding SEM image. It can be seen that the well-known homogenous tubular structure of carbon nanotube (Wang et al., 2020) is remarkably remained unchanged after being hybridized with egg albumin nanoparticles (Fig. 5B). The carbon nanotubes are interconnected with extended lengths in millimeters as shown in (Fig. 5B). Of special interest, nanosized egg albumin spheres of ~ 10 nm are shown to be incorporated and sparsely distributed within the carbon nanotubes, as represented by white circles, (Fig. 5C).

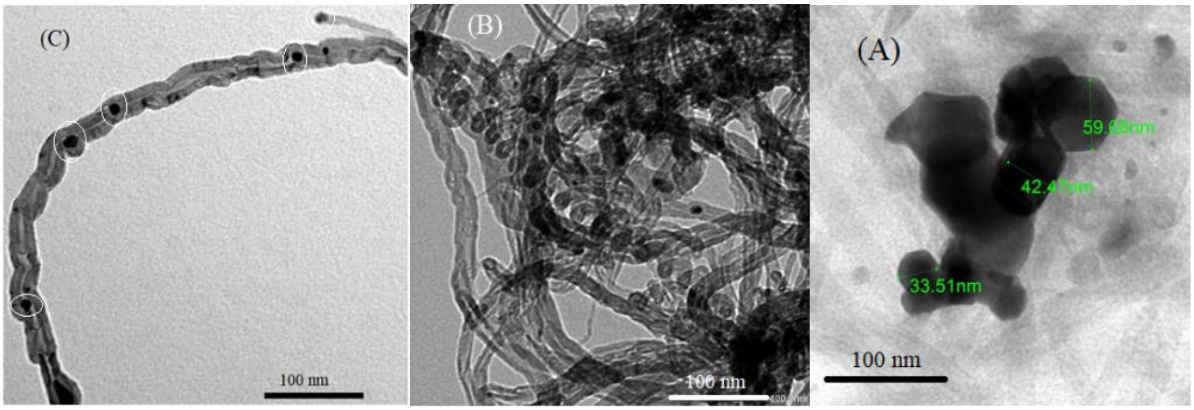

Fig. (5): TEM micrographs of: (A) EA-NPs and (B and C) EA/CNT nanocomposite.

2- The In vitro study

Determination of IC50 of CP on mammary gland breast cancer cell line (MCF7). IC50 was calculated from the following table.

Table (1): Shows IC50 value of CP on mammary gland breast cancer cell line (MCF7).

ID	Conc. ug/ml	O.D			Mean O.D	S.E	Viability %	Toxicity %	IC50
Mcf7	dilution	0.223	0.233	0.222	0.226	0.003512	100	0	
CP	1000	0.031	0.026	0.042	0.033	0.004726	14.60176991	85.39823009	482.03
	500	0.097	0.106	0.093	0.098667	0.003844	43.65781711	56.34218289	
	250	0.191	0.188	0.197	0.192	0.002646	84.95575221	15.04424779	
	125	0.222	0.23	0.227	0.226333	0.002333	100.1474926	0	
	62.5	0.225	0.224	0.229	0.226	0.001528	100	0	
	31.25	0.223	0.221	0.224	0.222667	0.000882	98.52507375	1.474926254	

3- In vivo study (The Toxicity Studies)

Determination of LD50 of CP&EA/CNT nanocomposite

Intraperitoneal injection of CP&EA/CNT nanocomposite in doses of 50, 250, 450, 650, 850, and 1050 mg/kg resulted in deaths of 0, 3, 7, 8, 9 and 10 respectively. The dose of CP&EA/CNT nanocomposite that killed half of the rats (LD50) was 375 mg/kg b.w. as in table 2.

Table (2): Shows rate of death of different doses of CP&EA/CNT nanocomposite.

Group Number	Dose(mg/kg)	No of animals/group	No of dead animals	Z	d	Z.d
1	50	10	0	1.5	250	375
2	250	10	3	5	250	500
3	450	10	7	7	250	1750
4	650	10	7	7.5	250	1875
5	850	10	8	9	250	2250
6	1050	10	10	0	250	0

Z = Half the sum of the dead rats from 2 successive groups.
d = the difference between 2 successive doses.

4- Biochemical analyses

4-1- Determination of kidney function (serum creatinine, urea, uric acid and BTP)

Serum Creatinine, urea, uric acid and BTP are markers of renal dysfunc-tion. Data was illustrated in table (3). Results indicated a significant increase (P<0.001) in creatinine, urea, uric acid and BTP levels of CP group with percent change (↑76.36%), (↑67.86), (↑94.52) and (↑960.0) respectively compared with control. On the other hand, creatinine, urea, uric acid and BTP values of CP&EA/CNT nanocomposite group showed a non-significant change compared with control.

Table (3): Data analyses of creatinine, urea, uric acid and BTP in three studied groups.

	Group I (control group)	Group II (CP group)	Group III (CP&EA/CNT composite group)	p
Creatinine				
Mean ± SE.	0.55 ± 0.02	0.97^{a} ± 0.12	0.64^{b} ± 0.04	0.016^{*}
Min. – Max.	0.51 – 0.59	0.80 – 1.20	0.60 – 0.72	
% Change from group I		↑76.36	↑16.36	
Urea				
Mean ± SE.	28.0 ± 1.53	47.0^{a} ± 1.53	34.67^{b} ± 2.33	0.001^{*}
Min. – Max.	25.0 – 30.0	44.0 – 49.0	31.0 – 39.0	
%Change from group I		↑67.86	↑23.82	
Uric acid				
Mean ± SE.	3.10 ± 0.06	6.03^{a} ± 0.15	3.50^{b} ± 0.29	$<0.001^{*}$
Min. – Max.	3.0 – 3.20	5.80 – 6.30	3.0 – 4.0	
%Change from group I		↑94.52	↑12.90	
B trace protein				
Mean ± SE.	0.55 ± 0.05	5.83^{a} ± 0.67	1.80^{b} ± 0.42	$<0.001^{*}$
Min. – Max.	0.45 – 0.63	4.60 – 6.90	1.20 – 2.60	
%Change from group I		↑960.0	↑227.3	

Data are expressed as Mean ± S.E for 8 rats/ group
p: p value for comparing between the three studied of healthy groups
a: Statistically significant with Group I; b: Statistically significant with Group II
*: Statistically significant at $p \leq 0.05$
Group I: control group; Group II: Healthy rats were injected with CP; Group III: Healthy rats were injected CP&EA/CNT nanocomposite group

4-2 Determination of glomerular injury (Level of serum Nephrin)

Nephrin is a novel biomarker of glomerular injury. Data was illustrated in table (4) and graphically represented in figure (21). Results indicated a significant increase (P< 0.001) in Nephrin level of CP group with percent change (↑155.5) compared with control group. While CP&EA/CNT nanocomposite group showed a non-significant change compared with control.

Table (4): Nephrin level in the three studied groups.

Nephrin	Group I (control group)	Group II (CP group)	Group III (CP&EA/CNT composite group)	p
Mean ± SE.	4.63 ± 0.41	11.83^{a} ± 0.73	7.0^{b} ± 0.58	$<0.001^{*}$
Min. – Max.	4.0 – 5.40	10.5 – 13.0	6.0 – 8.0	
% Change from group I		↑155.5	↑51.19	

Data are expressed as Mean ± S.E for 8 rats/ group

p: p value for comparing between the three studied of healthy groups.

a: Statistically significant with Group I;
b: Statistically significant with Group II
*: Statistically significant at $p \leq 0.05$
Group I: control group; Group II: Healthy rats were injected with CP; Group III: Healthy rats were injected CP&EA/CNT nanocomposite group

4-3- Assessment of inflammation (Level of IL8)

IL 8 is a biomarker of kidney inflammation. Data was illustrated in table (5) and graphically represented in figure (5). Results indicated a significant increase (P<0.001) in IL 8 level of CP group with percent change (↑113.6) compared with control group. On the other hand, IL8 values of CP&EA/CNT nanocomposite group decreased significantly in comparison with the group given CP only.

Table (5): Level of IL8 in three studied groups.

IL 8	Group I (control group)	Group II (CP group)	Group III (CP&EA/CNT composite group)	p
Mean ± SE.	36.67 ± 2.73	78.33[a] ± 4.41	54.0[ab] ± 2.08	<0.001*
Min. – Max.	33.0 – 42.0	70.0 – 85.0	50.0 – 57.0	
%Change from group I		↑113.6	↑47.26	

Data are expressed as Mean ± S.E for 8 rats/ group
p: p value for comparing between the three studied of healthy groups
a: Statistically significant with Group I; b: Statistically significant with Group II
*: Statistically significant at $p \leq 0.05$

Group I: control group; Group II: Healthy rats were injected with CP; Group III: Healthy rats were injected CP&EA/CNT nanocomposite group

4-4- Determination of tubulointerstitial injury (Level of serum NGAL).

NGAL is a biomarker of tubulointerstitial injury. Data was illustrated in table (18) and graphically represented in figure (23and 24). Results indicated a significant increase (P< 0.001) in NGAL level of CP group with percent change (↑322.4) compared with control group. On the other hand, NGAL values of CP&EA/CNT nanocomposite group decreased significantly in comparison with the group given CP only.

Table (13): Comparison of three studied groups according to NGAL parameter.

NGAL	Group I (control group)	Group II (CP group)	Group III (CP&EA/CNT composite group)	p
Mean ± SE.	14.44 ± 1.66	61.0[a] ± 3.79	27.33[ab] ± 2.33	<0.001*
Min. – Max.	11.25 – 16.84	55.0 – 68.0	23.0 – 31.0	
%Change from group I		↑322.4	↑89.27	

Data are expressed as Mean ± S.E for 8 rats/ group
p: p value for comparing between the three studied of healthy groups
a: Statistically significant with Group I;
b: Statistically significant with Group II
*: Statistically significant at $p \leq 0.05$
Group I: control group; Group II: Healthy rats were injected with CP; Group III: Healthy rats were injected CP&EA/CNT nanocomposite group

4-5 Histopathological Finding

Group I (control): It was found that, Kidney sections of control group showed normal renal glomeruli and tubules (Fig. 6A). Group II (CP Group): Kidney sections of rats injected with CP showed a marked congestion of the glomerular tufts, degeneration of the renal tubules lining epithelium and necrotic foci associated with mononuclear inflammatory cells infiltration (Fig. 6B). Group III (CP&EA/CNT nanocomposite Group): Kidney sections of rats injected with CP&EA/CNT nanocomposite showed marked decrease of the congestion of the glomerular tufts and of degenerative changes within the renal tubules (Fig. 6C).

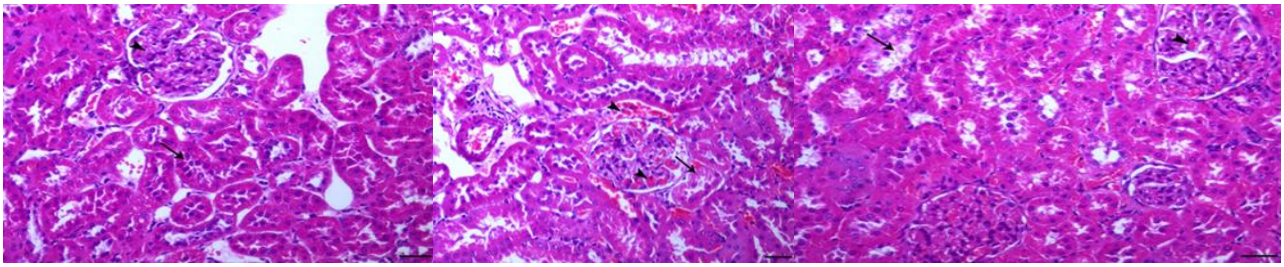

A **B** **C**

Figure (6): Kidney of normal animals showed normal histological structure of renal glomeruli and tubules (panel A); Kidney of rats injected with CP showed marked congestion of the glomerular tufts (arrowheads) and degeneration of the renal tubules lining epithelium (arrow; panel B), Kidney of rats injected with CP&EA/CNT nanocomposite showed marked decrease of the congestion of the glomerular tufts (arrowhead) and decrease of the degenerative changes within the renal tubules (arrow), (H&E, bar= 50 µm, X200).

DISCUSSION

Chemotherapy serves as one of the most important cancer treatment modalities and has been extensively used in clinic. However, conventional chemotherapeutics usually induce serious side effects such as hepatotoxicity, nephrotoxicity and cardiotoxicity due to their low half-lives in the blood and rapid distribution in healthy tissues and organs. Therefore, exploring and developing more efficient methods to enhance cancer chemotherapy is an urgent problem that must be solved. With the development of nanomedicine, multifunctional nanocarriers have showed a good application prospect in improving cancer chemotherapy (Wei et al., 2021).

Nanotechnology is a promising alternative to overcome different limitations in cancer therapy. Several nanoparticles (NPs; diameter 1–100 nm) carrying multiple drugs have been investigated regarding anticancer activities. NPs are characterized by the presence of high ligand density on the surface due to their high surface-area-to-volume ratio. They also increase local drug concentration by carrying the drug within and control its release upon reaching the targets (Shafei et al., 2017).

Cyclophosphamide (CP) is one of the oldest anticancer drugs. It is an alkylating agent of the oxazaphosphorin family, and has been used for a long time in chemotherapy (Sherif, 2020). It is widely used to treat various types of cancer including lymphoma, leukemia, breast, ovarian, colon and small-cell lung carcinomas (Iqubal et al., 2020; Zhao et al., 2020). However, the clinical use of this drug is restricted due to its adverse effects that include nephrotoxicity, hepatotoxicity, neurotoxicity, cardiotoxicity, immunotoxicity, urotoxicity, vomiting, nausea, alopecia, and bone marrow suppression (Caglayan et al., 2018; Taslimi et al., 2019).

CP is converted in the liver into two reactive metabolites, acrolein and phosphoramide. They interfere with tissues' antioxidant capacity with subsequent production of highly reactive oxygen free radicals. These radicals induce considerable structural damage by interacting with proteins' amino acids and DNA, producing irreversible DNA cross-links and leads to cell apoptosis (ALHaithloul et al., 2019).

Therefore, new manners are needed that can reduce the side effects of these drugs without interfering with their anticancer properties. Today more attention is being given to Nanoparticles as they are used as drug carriers and imaging to increase drug solubility, stability and control drug release and specific transport and reduce drug toxicity (Pavitra et al., 2019). The current study was constructed to evaluate the ameliorating effect of the newly synthesized cyclophosphamide +Egg albumin/carbon nanotubes nanocomposite against cyclophosphamide induced nephrotoxicity in rats. The physicochemical properties of the newly synthesized composite were also assessed.

The size and shape of (EA nanoparticles and EA/CNT) were characterized using transmission electron microscopy (TEM) by high resolution. The micrographs under low and high magnifications are demonstrated in (figure 1). SEM technique was applied to obtain information about the surface topography of the prepared nanomaterial as in (figure 2). The FT-IR spectroscopy is an effective tool to investigate the function group on the molecular level as in (figure 3). XRD is an analytical technique used to define and identify nano-materials and explain whether the sample materials are pure or contain impurities as in (figure 4).

The in vitro study (Cell viability assay) wherever the cytotoxic effect (IC50) of newly synthesized composite (CP&EA/CNT) and (CP only) on breast cancer cell line and colon cancer cell line were assessed using MTT assays. IC50 values revealed significant results of newly synthesized composite (CP&EA/CNT) on breast cancer cell line and colon cancer cell line (table 1). This study revealed that newly synthesized composite (CP&EA/CNT) was effective at inhibiting cell viability and proliferation. In determining a promising anticancer compound, the nature of the apoptotic mechanism that leads to cell death is essential. Cyclophosphamide is an antineoplastic in the class of alkylating agents and is used to treat various forms of cancer. Alkylating agents are so named because of their ability to add alkyl groups to many electronegative groups under conditions present in cells. They stop tumor growth by cross-linking guanine bases in DNA double-helix strands - directly attacking DNA. This makes the strands unable to uncoil and separate. As this is necessary in DNA replication, the cells can no longer divide. In addition, these drugs add methyl or other alkyl groups onto molecules where they do not belong which in turn inhibits their correct utilization by base pairing and causes a miscoding of DNA. Alkylating agents are cell cycle-nonspecific. Alkylating agents work by three different mechanisms all of which achieve the same end result - disruption of DNA function and cell death (Wormington et al., 2020).

The biochemical findings in the current in vivo experimental set up revealed that the increased serum creatinine, urea, uric acid and beta trace protein after CP administration table (3) could be due to their leakage into

the systemic circulation secondary to kidney damage and membrane permeability. BTP is a lipocalin glycoprotein and more sensitive indicator of glomerular filtration particularly in the 'creatinine-blind' range. Significant increase in serum creatinine is not observed in mild renal impairment, in contrast to serum BTP (Wajda et al., 2020). Our findings showed a marked increase in serum of B trace protein level of rats of group was injected with CP only (table 3). But group were injected with newly synthesized nanocomposite (CP&EA/CNT) significantly reduced B trace protein level. Our study is going with previous studies which revealed the utility of BTP to measure of kidney function and as biomarker for early detection of adverse outcomes and complications of AKI and chronic kidney disease (CKD) (Inker et al ; 2017; Wajda et al., 2020).

Nephrin is a slit diaphragm protein that is critical for glomerular filtration as it provides architectural support to podocytes. As nephrin is a glomerular-specific protein, monitoring of this biomarker might be more indicative of glomerular injury than other putative biomarkers (Heimlich et al., 2018). Our findings showed marked increase in serum of nephrin protein level of rats of group was injected with CP only as in (table1). But group was injected with newly synthesized nanocomposite (CP&EA/CNT) significantly reduced nephrin level. our results is agreement with earlier Report (J. Chen et al., 2019) which revealed that nephrin is a useful biomarker of glomerular maturation and injury and it is associated with acute kidney injury (AKI).

IL-8 is a proinflammatory cytokine produced by monocyte, neutrophil, endothelial, and epithelial cells, and it acts as a potent neutrophil activator and chemoattractant (de Fontnouvelle et al., 2017; Greenberg et al., 2018). Recent evidence demonstrated that the hallmark mechanism for CP-induced toxicity is the induction of proinflammatory cytokine associated with kidney inflammation. Activation of pro-inflammatory cytokines lead to elicit an inflammatory response (Mahmoud et al., 2015). Our findings showed a marked increase in IL 8 level of rats of group was injected with CP only as in (table 5). But group was injected with newly synthesized nanocomposite (CP&EA/CNT) significantly reduced IL8 level. Our study is going with previous studies which revealed activation of proinflammatory cytokine in response to oxidative stress, resulting in the stimulation of different inflammatory cytokines which cause tissue injury in CP-challenged rats (El-Kholy et al., 2017; El-Shabrawy et al., 2020).

NGAL is glycoprotein belonging to the lipocalin superfamily of proteins. Expression of NGAL mRNA increases more than 1000-fold in response to kidney injury and manifests as rapid elevation of urine and blood NGAL levels, making it useful as an early biomarker of kidney injury (Siddappa et al., 2019). Our findings showed a marked increase in NGAL level of rats of group was injected with CP only as in (table 6) and (Figure 6). But group was injected with newly synthesized nanocomposite (CP&EA/CNT) significantly reduced NGAL level. Our results is agreement with earlier Report (Zheng et al., 2020), which revealed the utility of NGAL to measures tubulointerstitial injury, diagnosis and evaluation of acute kidney injury.

Histological findings revealed that control group showed normal renal glomeruli and tubules (figure 33A) While CP treated groups showed a marked congestion of the glomerular tufts, degeneration of the renal tubules lining epithelium and necrotic foci associated with mononuclear inflammatory cells infiltration (figure 7B) as indicators of nephrotoxicity. But Kidney sections of rats injected with newly synthesized composite (CP&EA/CNT) showed marked decrease of the congestion of the glomerular tufts and of degenerative changes within the renal tubules (Fig. 7C). Our results is agreement with earlier Report (Seshan & Salvatore, 2021) which revealed that degeneration of the renal tubules lining epithelium and necrotic foci associated with mononuclear inflammatory cells infiltration are good indicators of nephrotoxicity.

In pilot study renal biomarkers and kidney sections showed the same results of study with healthy rats. Moreover, according to colon, DMH is a procarcinogen that undergoes metabolic activation in the liver through P450 monooxygenases (i.e. cytochrome (CYP) 2E1) and is converted into intermediates such as AOM, methylazoxymethanol acetate (MAM) and the highly reactive methyldiazonium and methyl ions. These metabolites produced in the liver are transported via bile or bloodstream to the colon. In both liver and colon, the methyldiazonium and methyl ions can alkylate DNA bases thus triggering colon carcinogenesis (Rosenberg et al., 2009; Siddique et al., 2017). Although the liver is considered the main metabolizing site for DMH, this carcinogen has also been proposed to be directly biotransformed by colonocytes and intestinal microbiota (Zhu et al., 2014; Caetanoa et al., 2020).

REFERENCES

1. Abdelmoneem, M. A., Mahmoud, M., Zaky, A., Helmy, M. W., Sallam, M., Fang, J. Y., Elkhodairy, K. A., & Elzoghby, A. O. Decorating protein nanospheres with lactoferrin enhances oral COX-2 inhibitor/herbal therapy of hepatocellular carcinoma. Nanomedicine, 2018; 13(19): 2377–2395. https://doi.org/10.2217/nnm-2018-0134
2. Aboushousha, T., Hammam, O., Aref, A., Kamel, A., Badawy, M., & Hamid, A. A. Tissue Profile of CDK4 and STAT3 as Possible Innovative Therapeutic Targets in Urinary Bladder Cancer. Asian Pacific Journal of Cancer Prevention, 2020; 21(2): 547–554.
3. Abraham, P., & Rabi, S. Protective effect of aminoguanidine against cyclophosphamide-induced

oxidative stress and renal damage in rats. Redox Report, 2011; 16(1): 8–14.
4. Al-Harthi, S., Lachowicz, J. I., Nowakowski, M. E., Jaremko, M., & Jaremko, Ł. Towards the functional high-resolution coordination chemistry of blood plasma human serum albumin. J. of Inorg. Bioc., 2019; 198: 110716.
5. Al-Harthi, S., Lachowicz, J. I., Nowakowski, M. E., Jaremko, M., & Jaremko, Ł. Towards the functional high-resolution coordination chemistry of blood plasma human serum albumin. Journal of Inorganic Biochemistry, 2019; 198: 110716.
6. ALHaithloul, H. A. S., Alotaibi, M. F., Bin-Jumah, M., Elgebaly, H., & Mahmoud, A. M. Olea europaea leaf extract up-regulates Nrf2/ARE/HO-1 signaling and attenuates cyclophosphamide-induced oxidative stress, inflammation and apoptosis in rat kidney. Biomedicine and Pharmacotherapy, 2019; 111: 676–685.
7. Amal, M. E., Hisham, M., Basma, A.., Emam, M., & Wanas, H. Protective effect of tolvaptan against cyclophosphamide- induced nephrotoxicity in rat models. Pharmacology Research & Perspectives, 2020; 8: 1–11.
8. Attallah, A. M., El-far, M. A., Omran, M. M., Mohamed, A., Attallah, K. A., Elbendary, M. S., Soliman, S. A., & Atwa, R. A. The efficiency of collagen III, metalloproteinase 1, carcinoembryonic antigen, and carbohydrate antigen 19, 9 for colon cancer diagnosis. Journal of Bioscience and Applied Research, 2019; 5(2): 167–175.
9. Ayza, M. A., Zewdie, K. A., Tesfaye, B. A., Wondafrash, D. Z., & Berhe, and A. H. Review. The Role of Antioxidants in Ameliorating Cyclophosphamide- Induced Cardiotoxicity. Oxidative Medicine and Cellular Longevity, 2020.
10. Bhatia, S. Natural Polymer Drug Delivery Systems. In Natural Polymer Drug Delivery Systems, 2016.
11. Boutin, A. T., Liao, W. T., Wang, M., Hwang, S. S., Karpinets, T. V., Cheung, H., Chu, G. C., Jiang, S., Hu, J., Chang, K., Vilar, E., Song, X., Zhang, J., Kopetz, S., Futreal, A., Wang, Y. A., Kwong, L. N., & DePinho, R. A. Oncogenic Kras drives invasion and maintains metastases in colorectal cancer. Genes and Development, 2017; 31(4): 370–382.
12. Caetanoa, B. F. R., Tablasb, M. B., Romualdoa, G. R., Rodriguesa, M. A. M., & Barbisan, L. F. Early molecular events associated with liver and colon sub-acute responses to 1,2-dimethylhydrazine: Potential implications on preneoplastic and neoplastic lesion development. Toxicology Letters, 2020; 329: 67–79.
13. Chen, J., Li, G., Wang, S., Hu, X., Sun, Y., Dai, X., Bai, Z., Pan, J., Li, X., Wang, J., & Li, Y. Urinary Nephrin as a Biomarker of Glomerular Maturation and Injury Is Associated with Acute Kidney Injury and Mortality in Critically Ill Neonates. Neonatology, 2019; 215025: 58–66.
14. Chen, L., Xiong, X., Hou, X., Wei, H., Zhai, J., Xia, T., Gong, X., Gao, S., Feng, G., Tao, X., Zhang, F., & Chen, W. Wuzhi capsule regulates chloroacetaldehyde pharmacokinetics behaviour and alleviates high-dose cyclophosphamide-induced nephrotoxicity and neurotoxicity in rats. Basic and Clinical Pharmacology and Toxicology, 2019; 125(2): 142–151.
15. Comparetti, E., Pedrosa, V. A., & Kaneno, R. Carbon Nanotube as a Tool for Fighting Cancer. Bioconjugate Chemistry, 2017; 29(October): 209–718. https://doi.org/10.1021/acs.bioconjchem.7b00563.
16. Cuce, G., Çetinkaya, S., Koc, T., Esen, H. I. H., Limandal, C., Balci, T., Kalkan, S., & Akoz, M. Chemoprotective effect of vitamin E in cyclophosphamide-induced hepatotoxicity in rats. Chemico-Biological Interactions, 2015; 232: 7–11.
17. Demaria, M., O'Leary, M. N., Chang, J., Shao, L., Liu, S., Alimirah, F., Koenig, K., Le, C., Mitin, N., Deal, A. M., Alston, S., Academia, E. C., Kilmarx, S., Valdovinos, A., Wang, B., De Bruin, A., Kennedy, B. K., Melov, S., Zhou, D.,Campisi, J. Cellular senescence promotes adverse effects of chemotherapy and cancer relapse. Cancer Discovery, 2017; 7(2): 165–176.
18. Deng, J., Zhong, Y., Wu, Y., Luo, Z., & Sun, Y. Redox Biology Carnosine attenuates cyclophosphamide-induced bone marrow suppression by reducing oxidative DNA damage. Redox Biology, 2018; 14: 1–6.
19. Deng, J., Zhong, Y., Wu, Y., Luo, Z., & Sun, Y. Redox Biology Carnosine attenuates cyclophosphamide-induced bone marrow suppression by reducing oxidative DNA damage. Redox Biology, 2018b; 14(August 2017): 1–6.
20. Dixit, R., Pandey, M., Tripathi, S. K., Dwivedi, A. N. D., & Shukla, V. K. Genetic mutational analysis of β-catenin gene affecting GSK-3β phosphorylation plays a role in gallbladder carcinogenesis: Results from a case control study. Cancer Treatment and Research Communications, 2020; 23: 100173.
21. El-Kholy, A. A., Elkablawy, M. A., & El-Agamy, D. S. Lutein mitigates cyclophosphamide induced lung and liver injury via NF-κB/MAPK dependent mechanism. Biomedicine and Pharmacotherapy, 2017; 92: 519–527. https://doi.org/10.1016/j.biopha.2017.05.103.
22. El-Moselhy, E. A., & Elrifai, A. W. Risk Factors of Lung Cancer Worldwide and in Egypt: Current Situation. J Oncopathol Clin Res, 2018; 2(2): 5. http://www.imedpub.com/journal-oncopathology-clinical-research/.
23. El-Shabrawy, M., Mishriki1, A., Attia1, H., Aboulhoda, B. E., Emam4, M., & Wanas, H. Protective effect of tolvaptan against cyclophosphamide- induced nephrotoxicity in rat models. Pharmacology Research & Perspectives, 2020; 8(May): 1–11. https://doi.org/10.1002/prp2.659.
24. Elgohary, M. M., Helmy, M. W., Abdelfattah, E. Z. A., Ragab, D. M., Mortada, S. M., Fang, J. Y., &

Elzoghby, A. O. Targeting sialic acid residues on lung cancer cells by inhalable boronic acid-decorated albumin nanocomposites for combined chemo/herbal therapy. Journal of Controlled Release, 2018; 285(July): 230–243. https://doi.org/10.1016/j.jconrel.2018.07.014.
25. Elzoghby, A. O., El-Lakany, S. A., Helmy, M. W., Abu-Serie, M. M., & Elgindy, N. A. Shell-crosslinked zein nanocapsules for oral codelivery of exemestane and resveratrol in breast cancer therapy. Nanomedicine, 2017; 12(24): 2785–2805. https://doi.org/10.2217/nnm-2017-0247.
26. Ghareeb, A. E., Moawed, F. S. M., & Kandil, E. I. Potential prophylactic effect of berberine against rat colon carcinoma induce by 1,2-Dimethyl hydrazine. Asian Pacific Journal of Cancer Prevention, 2018; 19(6): 1685–1690.
27. Ghorbani, F., Kokhaei, P., Ghorbani, M., & Eslami, M. Application of different nanoparticles in the diagnosis of colorectal cancer. Gene Reports, 2020; 21(October): 100896. https://doi.org/10.1016/j.genrep.2020.100896.
28. Grynberg, K., Ma, F. Y., & Nikolic-Paterson, D. J. The JNK signaling pathway in renal fibrosis. Frontiers in Physiology, 2017; 8(OCT): 1–12. https://doi.org/10.3389/fphys.2017.00829
29. Habib, B. A., Sayed, S., & Elsayed, G. M. Enhanced transdermal delivery of ondansetron using nanovesicular systems: Fabrication, characterization, optimization and ex-vivo permeation study-Box-Cox transformation practical example. European Journal of Pharmaceutical Sciences, 2018; 115: 352–361.
30. Hammouda, M. B., Ford, A. E., Liu, Y., & Zhang, J. Y. Disorders and Cancer. Cells, 2020; 1: 1–22.
31. Inker, L. A., Tighiouart, H., Coresh, J., Foster, M. C., Anderson, A. H., & Levey, A. S. GFR estimation using β-trace protein and β2-microglobulin in CKD. American Journal of Kidney Diseases, 2017; 176(10): 139–148.
32. Iqubal, A., Ali, M., Mahfuzul, M., & Kalam, A. Effect of nerolidol on cyclophosphamide-induced bone marrow and hematologic toxicity in Swiss albino mice. Experimental Hematology, 2020; 82: 24–32.
33. Iqubal, A., Ali, M., Mahfuzul, M., & Kalam, A. Effect of nerolidol on cyclophosphamide-induced bone marrow and hematologic toxicity in Swiss albino mice. Experimental Hematology, 2020; 82: 24–32.
34. Jiang, S., Zhang, Z., Yu, F., Zhang, Z., & Yang, Z. Ameliorative e ff ect of low molecular weight peptides from the head of red shrimp (Solenocera crassicornis) against cyclophosphamide-induced hepatotoxicity in mice. Journal of Functional Foods, 2020; 72: 104085.
35. Kabary, D. M., Helmy, M. W., Elkhodairy, K. A., Fang, J. Y., & Elzoghby, A. O. Hyaluronate/lactoferrin layer-by-layer-coated lipid nanocarriers for targeted co-delivery of rapamycin and berberine to lung carcinoma. Colloids and Surfaces B: Biointerfaces, 2018; 169: 183–194.
36. Karami, E., Behdani, M., & Kazemi-Lomedasht, F. Albumin nanoparticles as nanocarriers for drug delivery: focusing on antibody and nanobody delivery and albumin-based drugs. J of Drug Delivery Sci and Tech, 2020; 55: 101471.
37. Kunjeti, S. G., Anchieta, A., Subbarao, K. V., Koike, S. T., & Klosterman, S. J. Plasmolysis and vital staining reveal viable oospores of peronospora effusa in spinach seed lots. Plant Disease, 2016; 100(1): 59–65.
38. Kuzu, M., Kandemir, F. M., Yildirim, S., Kucukler, S., Caglayan, C., & Turk, E. Morin attenuates doxorubicin-induced heart and brain damage by reducing oxidative stress, inflammation, and apoptosis. Biomedicine and Pharmacotherapy, 2018; 106(June): 443–453.
39. Lee, B. C., & Soh, K. S. Visualization of Acupuncture Meridians in the Hypodermis of Rat Using Trypan Blue. JAMS Journal of Acupuncture and Meridian Studies, 2010; 3(1): 49–52.
40. Li, Z., Shi, Y., Ding, Y., & Le, G. Dietary oxidized tyrosine (O‐Tyr) stimulates TGF‐β1‐induced extracellular matrix production via the JNK / p38 signaling pathway in rat kidneys. Amino Acids, 2017; 49(2): 241–260.
41. Liu, Y., Shen, P., Zhou, Y., Tang, L., & Chai, H. c‐Jun N‐terminal kinase/transforming growth factor‐β/Smad3 pathway: Is it associated with endoplasmic reticulum stress‐mediated renal interstitial fibrosis? Molecular Medicine Reports, 2019; 20(1): 755–762.
42. Mahajan, S., Patharkar, A., Kuche, K., Maheshwari, R., Deb, P. K., Kalia, K., & Tekade, R. K. Functionalized carbon nanotubes as emerging delivery system for the treatment of cancer. International Journal of Pharmaceutics, 2018; 548(1): 540–558.
43. Mahmoud, A. M., & Nrf, I. Á. P. Á. 18 b - Glycyrrhetinic acid exerts protective effects against cyclophosphamide-induced hepatotoxicity : potential role of PPAR c and Nrf2 upregulation. Genes & Nutr, 2015; 10: 1–13.
44. Mahmoud, A. M., Germoush, M. O., Alotaibi, M. F., & Hussein, O. E. Possible involvement of Nrf2 and PPAR g up-regulation in the protective effect of umbelliferone against cyclophosphamide-induced hepatotoxicity. Biomedicine et Pharmacotherapy, 2017; 86: 297–306.
45. Nafee, N., Makled, S., & Boraie, N. Nanostructured lipid carriers versus solid lipid nanoparticles for the potential treatment of pulmonary hypertension via nebulization. European Journal of Phar Sci, 2018; 125: 151–162.
46. Nasr, M. Development of an optimized hyaluronic acid-based lipidic nanoemulsion co-encapsulating two polyphenols for nose to brain delivery. Drug Delivery, 2016; 23(4): 1444–1452.

47. Noorani, M., Azarpira, N., Karimian, K., & Heli, H. Erlotinib-loaded albumin nanoparticles: A novel injectable form of erlotinib and its in vivo efficacy against pancreatic adenocarcinoma ASPC-1 and PANC-1 cell lines. International Journal of Pharmaceutics, 2017; 531(1): 299–305.
48. Pandurangan, A. kumar, Divya, T., Kumar, K., Dineshbabu, V., Velavan, B., & Sudhandiran, G. Colorectal carcinogenesis: Insights into the cell death and signal transduction pathways: A review. World Journal of Gastrointestinal Oncology, 2018; 10(9): 244–259.
49. Patton, Crouch, C. J. and, & SR. Spectrophotometric and Kinetics Investigation of the Berthelot Reaction for the Determination of Ammonia. Analytical Chemistry, 1977; 49(3): 464–469.
50. Pavitra, E., Dariya, B., Srivani, G., Kang, S. M., Alam, A., Sudhir, P. R., Kamal, M. A., Raju, G. S. R., Han, Y. K., Lakkakula, B. V. K. S., Nagaraju, G. P., & Huh, Y. S. Engineered nanoparticles for imaging and drug delivery in colorectal cancer. Seminars in Cancer Biology, 2019; 1–14.
51. Ruano, P., Delgado, L. L., Picco, S., Villegas, L., Tonelli, F., Merlo, M., Rigau, J., Diaz, D., & Masuelli, M. We are IntechOpen , the world ' s leading publisher of Open Access books Built by scientists , for scientists TOP 1 %. Intech, tourism, 2016; 13.
52. Ruano, P., Delgado, L. L., Picco, S., Villegas, L., Tonelli, F., Merlo, M., Rigau, J., Diaz, D., & Masuelli, M. We are IntechOpen, the world' s leading publisher of Open Access books Built by scientists , for scientists TOP 1 %. Intech, tourism, 2016; 13.
53. Saeed, Y., Wang, J. Q., & Zheng, N. Furosine induces DNA damage and cell death in selected human cell lines: a strong toxicant to kidney Hek-293 cells. Food Science and Biotechnology, 2017; 26(4): 1093–1101.
54. Sallam, M. A., & Elzoghby, A. O. Flutamide-Loaded Zein Nanocapsule Hydrogel, a Promising Dermal Delivery System for Pilosebaceous Unit Disorders. AAPS PharmSciTech, 2018; 19(5): 2370–2382.
55. Sanad, R. A. B., & Abdel-Bar, H. M. Chitosan–hyaluronic acid composite sponge scaffold enriched with Andrographolide-loaded lipid nanoparticles for enhanced wound healing. In Carbohydrate Polymers, 2017; 173.
56. Sarhan, W. A., & Azzazy, H. M. Apitherapeutics and phage-loaded nanofibers as wound dressings with enhanced wound healing and antibacterial activity. Nanomedicine, 2017; 12(17): 2055–2067.
57. Schultz, A. No Title Uric acid. Clin. Chem, The CV Mosby Co. St. Louis. Toronto. Princeton, 1984; 1261--1266.
58. Searle, & L, P. No Title The Berthelot or indophenol reaction and its use in the analytical chemistry of nitrogen. A review. Analyst, 1984; 109(5): 549--568.
59. Shaat, H., Mostafa, A., Moustafa, M., Gamal-Eldeen, A., Emam, A., El-Hussieny, E., & Elhefnawi, M. Modified gold nanoparticles for intracellular delivery of anti-liver cancer siRNA. International Journal of Pharmaceutics, 2016; 504(1–2): 125–133. https://doi.org/ 10.1016/j.ijpharm.2016.03.051.
60. Siddique, A. I., Mani, V., Arivalagan, S., Susan, N., & Namasivayam, N. Asiatic acid attenuates pre-neoplastic lesions, oxidative stress , biotransforming enzymes and histopathological alterations in 1 , 2-dimethylhydrazine-induced experimental rat colon carcinogenesis. Toxicology Mechanisms and Methods, 2017; 6516.
61. Sinanoglu, O., Yener, A. N., Ekici, S., Midi, A., & Aksungar, F. B. The protective effects of spirulina in cyclophosphamide induced nephrotoxicity and urotoxicity in rats. Urology, 2012; 80(6): 1392.e1-1392.e6. https://doi.org/10 .1016/j. urology.2012.06.053.
62. Sripriyalakshmi, S., Anjali, C. H., George Priya Doss, C., Rajith, B., & Ravindran, A. BSA nanoparticle loaded atorvastatin calcium - A new facet for an old drug. PLoS ONE, 2014; 9(2): 1–10.
63. Tabata, T., Sugiyama, N., Otsuki, Y., & Kondo, Y. Interleukin‐24 is a novel diagnostic biomarker for the severity of acute kidney injury. Medical Molecular Morphology, 2020; 53(2): 115–123.
64. Taslimi, P., Kandemir, F. M., Demir, Y., İleritürk, M., Temel, Y., Caglayan, C., & Gulçin, İ. The antidiabetic and anticholinergic effects of chrysin on cyclophosphamide-induced multiple organ toxicity in rats: Pharmacological evaluation of some metabolic enzyme activities. Journal of Biochemical and Molecular Toxicology, 2019; 33(6): 1–7. https://doi.org/10.1002/jbt.22313.
65. Twentyman PR, & Luscombe M. A study of some variables in a tetrazolium dye (MTT) based assay for cell growth and chemosensitivity. British Journal of Cancer, 1987; 56(3): 279–285.
66. Varanko, A., Saha, S., & Chilkoti, A. Recent trends in protein and peptide-based biomaterials for advanced drug delivery. JAdvanced Drug Delivery Reviews, 2020; 24: 91–98.
67. Voelcker, G. Causes and possibilities to circumvent cyclophosphamide toxicity. Anti-Cancer Drugs, 2020; 31: 617–622.
68. Wajda, J., Dumnicka, P., Sporek, M., Maziarz, B., Kolber, W., Ząbek-Adamska, A., Ceranowicz, P., Kuźniewski, M., & Kuśnierz-Cabala, B. Does Beta-Trace Protein (BTP) Outperform Cystatin C as a Diagnostic Marker of Acute Kidney Injury Complicating the Early Phase of Acute Pancreatitis? Journal of Clinical Medicine, 2020; 9(1): 205.
69. Wang, X., Sharif, F., Liu, X., Licht, G., Lefler, M., & Licht, S. Magnetic carbon nanotubes: Carbide nucleated electrochemical growth of ferromagnetic CNTs from CO2. Journal of CO2 Utilization, 2020; 40: 101218.

70. Wolski, P., Wojton, P., Nieszporek, K., & Panczyk, T. Interaction of Human Telomeric i-Motif DNA with Single-Walled Carbon Nanotubes: Insights from Molecular Dynamics Simulations. Journal of Physical Chemistry B, 2019; 123(49): 10343–10353.
71. Wu, H., Shi, H., Zhang, H., Wang, X., Yang, Y., Yu, C., Hao, C., Du, J., Hu, H., & Yang, S. Prostate stem cell antigen antibody-conjugated multiwalled carbon nanotubes for targeted ultrasound imaging and drug delivery. Biomaterials, 2014; 35(20): 5369–5380. https://doi.org/10.1016 /j.biomaterials.2014.03.038.
72. Zhang, J. J., Lan, T., & Lu, Y. Molecular Engineering of Functional Nucleic Acid Nanomaterials toward In Vivo Applications. Advanced Healthcare Materials, 2019; 8(6): 1–24.
73. Zhao, Y., Cai, C., Liu, M., Zhao, Y., Pei, W., Chu, X., Zhang, H., Wang, Z., & Han, J. Colloids and Surfaces B : Biointerfaces An organic solvent-free technology for the fabrication of albumin-based paclitaxel nanoparticles for effective cancer therapy. Colloids and Surfaces B: Biointerfaces, 2019; 183(May): 110394.
74. Zhao, Y., Yan, Y., Zhou, W., Chen, D., Huang, K., Yu, S., Mi, J., & Lu, L. E ff ects of polysaccharides from bee collected pollen of Chinese wolfberry on immune response and gut microbiota composition in cyclophosphamide- treated mice. Journal of Functional Foods, 2020; 72.
75. Zheng, Y., Guan, H., Zhou, X., Xu, Y., Fu, C., Xiao, J., & Ye, Z. The association of renal tubular inflammatory and injury markers with uric acid excretion in chronic kidney disease patients. International Urology and Nephrology, 2020; 52(5): 923–932.